Journal Pre-proof

Rapid microwave-assisted bulk production of high-quality reduced graphene oxide for lithium ion batteries

Jianshen Wu , Jiawei Zhao , Bala Vaidhyanathan , Hongtao Zhang , Aashu Anshuman , Avias Nare , Sina Saremi-Yarahmadi

PII: S2589-1529(20)30249-0
DOI: https://doi.org/10.1016/j.mtla.2020.100833
Reference: MTLA 100833

To appear in: *Materialia*

Received date: 21 March 2020
Accepted date: 15 July 2020

Please cite this article as: Jianshen Wu , Jiawei Zhao , Bala Vaidhyanathan , Hongtao Zhang , Aashu Anshuman , Avias Nare , Sina Saremi-Yarahmadi , Rapid microwave-assisted bulk production of high-quality reduced graphene oxide for lithium ion batteries, *Materialia* (2020), doi: https://doi.org/10.1016/j.mtla.2020.100833

Rapid microwave-assisted bulk production of high-quality reduced graphene oxide for lithium ion batteries

Jianshen Wu[a], Jiawei Zhao[a], Bala Vaidhyanathan[a]*, Hongtao Zhang[a], Aashu Anshuman[a], Avias Nare[a], Sina Saremi-Yarahmadi[a]

[a] Department of Materials, Loughborough University, Loughborough, Leicestershire, LE11 3TU, U.K.

* **Corresponding author**

Bala Vaidhyanathan

Tel./Fax: + 44 (0) 1509 223152.

E-mail address: B.Vaidhyanathan@lboro.ac.uk

Department of Materials, Loughborough University, Loughborough, Leicestershire, LE11 3TU, U.K.

Graphical abstract

Abstract

Graphene-based advanced electrodes with improved electrochemical properties have received increasing attention for use in lithium ion batteries (LIBs). The conventional synthesis of graphene via liquid phase exfoliation or chemical reduction of graphene oxide (GO) approaches, however, either involves prolonged processing or leads to the retainment of high-concentration oxygen functional groups (OFGs). Herein, bulk synthesis of high-quality reduced graphene oxide using microwave irradiation (MWrGO) within few seconds is reported. The electromagnetic interaction of GO with microwaves is elucidated at molecular level using reactive molecular dynamic simulations. The simulation suggests that higher power microwave irradiation results in significantly less retainment of OFGs and the formation of structural voids. The synthesized MWrGO samples are thoroughly characterized in terms of structural evolution and physicochemical properties. Specifically, a modified $I_D/I_{G\text{-}in}$ ratio metric for Raman spectrum, wherein the intensity contribution of D' peak is deducted from the apparent G peak, is proposed to investigate the structural evolution of synthesized MWrGO, which yields a more reliable evaluation of structural disorder over traditional I_D/I_G ratio. Li-ion half-cell studies demonstrate that the MWrGO is an excellent candidate for usage as high capacity anode (750.0 mAh g^{-1} with near-zero capacity loss) and high-performance cathode (high capacity retention of ~70% for $LiCoO_2$ at 10 C) for LIBs.

Keywords: Microwave-assisted synthesis; graphene; Li ion battery; Molecular dynamics simulations; Raman spectroscopy.

1. Introduction

Rapid production of high-quality reduced graphene oxide (rGO) with less OFGs and large lateral dimensions is pursued worldwide owing to the fascinating intrinsic properties of graphene such as highly flexible but mechanically robust structure, excellent electronic conductivity, and massive theoretical specific surface area (2630 $m^2 g^{-1}$) [1, 2]. High-quality rGO has found widespread applications in energy generation/storage devices, especially LIBs [3-5]. Although chemical vapor deposition (CVD) and mechanical exfoliation approaches have been well developed to produce graphene, their outcomes are generally unsatisfactory due to the high cost ~~and the tedious process involved~~. The alternative approach to produce graphene is reduction of GO using chemical reducing agents or conventional thermal treatment. Nevertheless, the synthesized rGO possesses high concentration of OFGs and low carbon-to-oxygen atomic ratio (C/O). In order to produce high-quality rGO in a rapid and low cost manner, reduction of GO using microwave irradiation is recently explored because it simultaneously combines the advantages of low cost by Hummer's method and super-fast volumetric heating by microwave irradiation [6-8].

Initially, microwave-assisted reduction of GO was accomplished in organic solvents, e.g. oleylamine, and *N,N*-dimethylformamide [9, 10]. However, the extent of reduction of GO in organic solvents was inferior because of the low boiling points of organic solvents (generally <300 °C). It was reported that the temperature required to effectively reduce GO was ~1050 °C in argon atmosphere [11] and 800 °C in hydrogen atmosphere [12], which were difficult to achieve in organic solvents. Additionally, the rGO tends to aggregate to become large particulates in solvents, which ultimately impairs the attainable properties of rGO. Afterwards, much efforts have been devoted to microwave-assisted reduction of GO in solid powder form [3, 4, 13, 14]. The first direct microwave-assisted reduction of solid-state GO was achieved by Ruoff in a domestic microwave oven [13], Following that, the microwave-driven reduction process of solid-state GO was optimized by using an array of microwave secondary susceptors, e.g. graphene, carbon black or graphite. They were employed to enhance microwave absorption and trigger super-heating to facilitate the reduction of surrounding GO powder [3, 4, 15, 16]. However, it has been revealed that the reduction reaction mainly occurred in places where the microwave susceptors were present, thereby resulting in non-uniform reduction of GO [3].

To overcome this issue, Voiry optimized the microwave absorption process by annealing the GO powder at 300 °C prior to microwave irradiation [17]. This pre-annealing treatment can convert entire GO from a poor microwave absorber to an extraordinary microwave absorber due to the partial restoration of the π-π conjugated network of GO. This led to the intensive volumetric microwave heating and uniform microwave reduction [3, 15, 17]. Whilst number of studies have been made to produce microwave-assisted rGO, most of the studies so far are focused on the fixed power microwave synthesis. Therefore, the effects of varied microwave power on the structural evolution and the extent of reduction of GO remain unknown and need to be explored.

Following Voiry's work, Chaban theoretically studied the microwave-assisted reduction process of GO using reactive molecular dynamics (RMD) and concluded that the different oxygen-containing

groups were deoxygenized at very different temperature regimes [18]. Though their work provided a fundamental understanding of electromagnetic interaction of GO with microwaves at a molecular level, no such reports are available on microwave interaction of annealed GO. Further, whilst the pioneering work of Chaban shed some light on the reaction mechanisms of reduction of GO using microwaves, it did not consider the effect of localized microwave heating generated at OFGs – the current work fills this extremely vital gap in understanding.

Despite that commercial LIBs have currently achieved grand successes as power sources for portable electronic devices, the commonly used graphite anode and $LiCoO_2$-based cathode cannot satisfy the demanding requirements of the advanced LIBs due to the low capacity and the inferior rate capability, respectively. Therefore, the electrochemical properties of LIBs can be improved using MWrGO because it is regarded as a promising electroactive material to replace traditional graphite in anode and as a conductive additive in cathode. However, with MWrGO as anode, only limited capacity was obtained, e.g. 400 mAh g^{-1} at 0.1 C for few-layered MWrGO [19]. The low capacity was probably attributed to the inefficient reduction of GO without pre-annealing treatment, which will be addressed in the work. On the other hand, the rate capability of $LiCoO_2$/rGO cathode, in which rGO was produced using thermal/chemical reduction approaches, is still poor. For instance, when thermally prepared rGO was used as conductive additive in $LiCoO_2$-based cathode, the capacity of $LiCoO_2$/rGO cathode drastically declined to ~0 mAh g^{-1} at 2 C [20]. The low capacity at high current rate was related to the inferior electronic conductivity of rGO caused by inefficient thermal reduction. To date, the effect of rGO prepared using microwave irradiation, i.e. MWrGO, on the electrochemical properties of $LiCoO_2$-based cathode has not been reported and will be further examined in this work.

Herein, the GO prepared using modified Hummer's method was first pre-annealed at 250 °C to restore partial graphitic structures before being subjected to microwave irradiation at different powers (300, 500, and 800 W) (Fig. S1). The microwave-synthesized products of annealed GO are denoted as MWrGO-X where X represents the microwave power. It is found that the microwave-assisted reduction process can be completed within few seconds at the super-fast heating rate of 30,000 °C min^{-1}. For comparative study of the impact of pre-annealing treatment on microwave absorption, GO without pre-annealing treatment (denoted as unannealed GO) was subjected to microwave irradiation and was compared with annealed GO. A computer simulation using RMD was used to mimic the thermal deoxygenation process of OFGs at different microwave powers by considering the microwave localized heating of functionalized carbon atoms. The simulation results suggested that different microwave powers could be used to tailor the quality of MWrGO – a unique trait that can be exploited based on need. The obtained MWrGO-800W exhibited a highly porous structure, high C/O ratio (≈14.29), high surface area (310.24 m^2 g^{-1}) and high electronic conductivity (761.4 S m^{-1}). For LIBs application, the anode made of MWrGO-800W delivered a high discharge capacity of 750.0 mAh g^{-1} at 0.2 A g^{-1} with near-zero capacity loss after 100 cycles. Additionally, the LCO-based cathode with MWrGO-800W as conductive additive was shown to exhibit an improved capacity retention and rate capability compared to the counterpart containing carbon nanotube (CNT).

2. Experimental

2.1. Synthesis of MWrGO

The GO suspension was prepared using a modified Hummer's method [21, 22] and was used to produce GO beads in $CaCl_2$ coagulation bath (See the Supporting information) [23]. Afterwards, the as-prepared GO was annealed at 250 °C for 1 hour in argon atmosphere to obtain annealed GO. The annealed GO was placed inside a microwave transparent quartz reactor, which was flushed with argon gas for 10 min to create an inert atmosphere. Microwave irradiation was performed at powers of 300, 500, and 800 W using a customized microwave oven (WaveDOM 7020, 2.45 GHz frequency). For comparison, as-prepared GO without the annealing treatment (denoted as unannealed GO) was exposed to 800 W microwave irradiation in identical argon atmosphere. Upon microwave irradiation, the real-time temperature profiles across annealed GO and unannealed GO were monitored using thermal imaging camera (FLIR-A655sc, Sweden).

2.2. Characterizations

The morphologies of MWrGO was investigated using field emission gun scanning electron microscopy (FEGSEM; JEOL-7800F) and high-resolution transmission electron microscopy (HR-TEM; FEI-Tecnai) equipped with Supertwin symmetric lenses. The structure and composition were characterized using Micron-Raman spectroscopy (Horiba Jobin-Yvon, 514 nm), X-ray diffraction (XRD; Bruker D2), Fourier transform infrared spectroscopy (FTIR; Shimadzu 8400S), thermogravimetric analysis (TGA; TA Instruments Q5000IR), X-ray photoelectron spectroscopy (XPS; Thermo Scientific, Al-Kα *hv*=1486.6 eV). The isotherms of N_2 physisorption were recorded (Tristar^{TM} 3000) and was used to calculate the S_{BET} and the pore size distribution. Electronic conductivity was measured on dense pellets using a four-probe method (Keithley 580).

2.3. Simulation

Simulations were carried out on LAMMPS [24] and the visualization was obtained using OVITO [25]. As supported by Car-Parrinello MD, ReaxFF was used to govern the dynamics [26, 27]. Two simulation scenarios, i.e. direct heating and microwave localized heating, were performed on GO with a timestep of 0.1 fs. For direct heating simulation, GO sheet which consisted of 1073 carbon atoms with designated 30 oxygen functional groups (OFGs) (hydroxyl groups, epoxide groups, and carbonyl groups) was simulated in a large cell. Direct heating was achieved using Nose-Hover thermostat from 273 to 3000 K in 500 ps. The first three reduction events of each OFGs were recorded to calculate the average reduction temperatures. For microwave localized heating simulation, only functionalized carbon atoms were heated up because microwaves were absorbed only by charged carbon atoms (with a threshold charge >0.08 e). Whereas the other carbon atoms were freely simulated (Fig. S3). In this simulation, the annealed GO sheet with 10.2 nm × 9.8 nm was constructed with C/O=5.04. The charged carbon atoms were coupled by a thermostat heating of 3.454 K ns^{-1}, 9.454 K ns^{-1} and 15.454 K ns^{-1} to mimic different microwave powers, respectively.

2.4. Electrochemical measurements

2.4.1. The preparation of MWrGO anode.

The slurry of 60 wt% MWrGO and 40 wt% polyvinylidene fluoride (PVDF) was prepared using *N*-methyl pyrrolidinone (NMP, 99%) and was blade cast on Cu foils, followed by drying at 100 °C

overnight. Afterwards, the dried electrode was roll pressed and punched out (8 mm discs). The mass loading was ~0.2 mg cm^{-2}.

2.4.2. The preparation of cathode.

The stoichiometric amounts of Co_3O_4 (≥99%, Sigma) and Li_2CO_3 (≥99%, Fisher) were ball milled at 200 rpm for 16 hours with the ball-to-powder ratio of 10:1, followed by calcination at 850 °C for 5 hours to prepare $LiCoO_2$ (LCO). The slurry of 91% LCO, 1 wt% MWrGO-800W and 8 wt% PVDF was prepared for MWrGO-containing cathode (LCO-MWrGO) and the slurry of 89 % LCO, 3 wt% CNT and 8 wt% PVDF was prepared for CNT-containing cathode (LCO-CNT) using NMP. The slurries were blade cast on Al foils, followed by drying at 100 °C overnight. Afterwards, the dried electrodes were roll pressed and punched out (8 mm discs). The mass loading was ~3.1 mg cm^{-2} for LCO-MWrGO and ~3.0 mg cm^{-2} for LCO-CNT.

All the working electrodes prepared above were assembled in 2032 type coin cells with lithium metal as counter electrode in Ar-filled glove box (MBraun). Celgard 2325 membrane was used as separators and the electrolyte of 1.0 M $LiPF_6$ in ethylene carbonate/dimethyl carbonate (1:1 v/v) was used. All the cells were conditioned for 1 day and galvanostatically charged/discharged using multi-channel battery tester (Neware, BTS-4008). Cyclic voltammetry (CV) test was performed for MWrGO anode at 0.1 mV s^{-1} in 0.01-2.5 V (BioLogic VSP). Electrochemical impedance spectroscopy (EIS) was conducted on LCO-based cathodes in the frequency range 10 kHz–0.01 Hz with an AC amplitude of 5 mV.

3. Results and discussion

3.1 The enhanced microwave absorption of GO by annealing treatment

Fig. 1a depicts the effect of pre-annealing treatment on the microwave absorption of unannealed GO and annealed GO. In sharp contrast with the highest temperature of ~160 °C achieved on the unannealed GO, the annealed GO could be heated up to ~670 °C within few milliseconds due to the boosted microwave coupling capability caused by partial restoration of conjugated graphitic structure. The modified Hummer's method introduced OFGs on the basal planes of GO, which cleaved the defect-free conjugated structure down to tiny polyaromatic islands [3]. Those polyaromatic islands created inter-boundaries along the vicinity of the OFGs and thus confined the transportation of π electrons within delimited regions. Consequently, the π electrons were hard to be driven by the E-field component of the electromagnetic microwaves to transport over a long range to generate enough Joule heating to effectively reduce GO. Fortunately, GO is thermodynamically unstable due to the incorporated -OH and -C=O groups [3, 10]. The pre-annealing treatment of GO at 250 °C can remove the -OH and -C=O groups and thus eliminate the inter-boundaries of defective regions, leading to partial restoration of the conjugated structures. This enabled the transportation of π electrons over a longer distance and generated significant amounts of Joule heating, yielding a remarkable heating rate of 30,000 °C min^{-1} for annealed GO. This value was far greater than that of 2,000 °C min^{-1} achieved in conventional rapid thermal reduction method [11]. This superfast heating rate was the direct result of intense microwave absorption and efficient conversion from microwave energy to thermal energy [11]. Furthermore, the obtained high temperature (~670 °C) of annealed GO was also believed to result in the localized deoxygenation of OFGs.

During microwave irradiation, it is also interesting to find that strong arcing was observed on annealed GO after just 1-3s of microwave irradiation (Movie S1 and Fig. S4), whereas no arcing was observed on unannealed GO after even 60 s. The occurrence of microwave-induced arcing may be ascribed to the congregation of π electrons at the sharp sites on graphene planes, which led to the ionization of the surrounding gas [15]. During microwave irradiation of annealed GO, the residual OFGs were locally heated and deoxygenated, which further eliminated the inter-boundaries around OFGs and enabled more π electrons to transport over a longer distance. In this scenario, a higher concentration of π electrons was built up at sharp sites, such as plane edges or defective points, resulting in the formation of intense electrostatic field [28]. The induced electrostatic field was likely to ionize the surrounding gas through electron excitation, which was perceived as electric arcing. It is also believed that the microwave reduction of GO was a self-accelerating deoxygenation process because the freshly formed MWrGO themselves became additional microwave absorption regions and in turn converted more microwave energy to thermal energy to remove the residual OFGs.

The morphologies of unannealed GO and annealed GO were characterized using FEGSEM (Fig. 1b-c). The original microstructure of unannealed GO was observed to be quite compact and dense (Fig. 1b). After the annealing treatment at 250 °C, a highly porous structure was formed (Fig. 1c), which was accompanied with a remarkable volume expansion of GO (Fig. S5). The formation of porous structure was ascribed to vigorous release of gases, like CO, CO_2, and H_2O, during annealing treatment [14, 18]. Since the decomposition rate of OFGs exceeded the diffusion rate of the gases through the GO, the released gases were initially trapped in the GO and resulted in a rapid pressure build-up. Once the internal pressure reached the threshold of Van der Waals forces, the graphitic layers were violently exfoliated and concurrently resulted in the formation of highly porous structure.

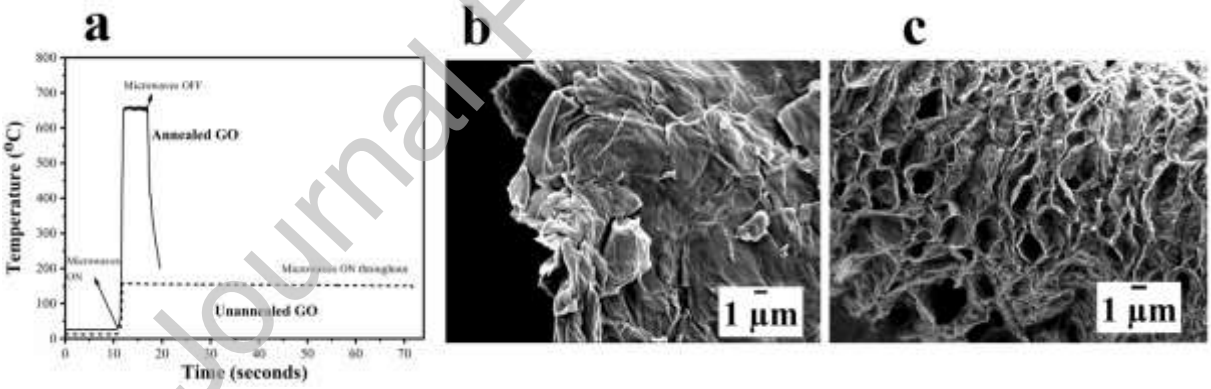

Fig. 1. (a) Time-temperature profiles of annealed and unannealed GO by 800 W microwave irradiation. The heating rate is ~30,000 °C min^{-1} for annealed GO and ~2000 °C min^{-1} for unannealed GO. (b-c) FEGSEM images of (b) unannealed GO and (c) annealed GO.

The morphology of MWrGO-800W flakes were characterized using HR-TEM. The MWrGO-800W featured a distinctively transparent and wrinkled surface with some stacking regions at the edges (Fig. 2a). Furthermore, the closer microscopic examination (Fig. 2b) shows well-resolved lattice fringes, indicative of significant exfoliation of microwave reduced GO. The inset in Fig. 2b shows sharp electron diffraction pattern with two sets of symmetric hexagonal peaks at the edge region, further indicating the well-crystallized hexagonal graphitic structure. Noticeably, the higher intensity of the first-order spots over the second-order spots implied the presence of single layer graphene.

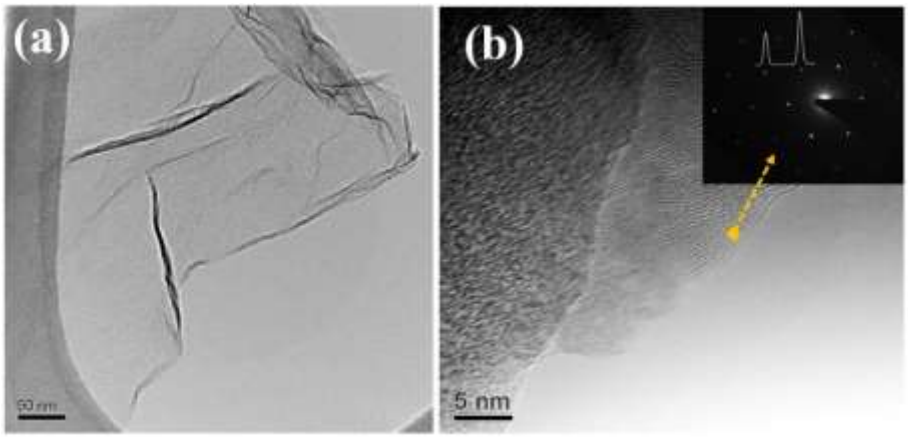

Fig. 2. HR-TEM images of MWrGO-800W at (a) low and (b) high magnification. The electron diffraction pattern is given in the inset, along with the diffraction intensity profiles of (11$\bar{2}$0) and (1$\bar{1}$00).

3.2. The microwave interaction simulation

RMD simulation can provide insights into the atomistic information regarding transformations and deoxygenation of OFGs during microwave irradiation. Two simulation scenarios, i.e. direct heating and microwave localized heating, were carried out. In the direct heating simulation, the deoxygenation temperatures of different OFGs were presented in Fig. 3a. From the simulation results, it is concluded that the hydroxyl groups were decomposed from GO sheets at roughly 1200 K, followed by removal of epoxide, and carbonyl groups above 2200 K. The decomposition of hydroxyl groups at lower temperature was supported by previous research [29, 30]. Based on the simulation results, the decomposition mechanisms of hydroxyl, epoxide, and carbonyl groups are proposed in Fig. 3b-d. The hydroxyl group was decomposed from carbon skeleton by breaking the C-OH bond during microwave irradiation and then was released as a hydroxyl free radical (Fig. 3b). As for the decomposition of epoxide group, the two C-O bonds sequentially broke, and an oxygen atom was then released, as illustrated in Fig. 3c. Notably, if two epoxide groups are linked by a carbon-carbon bond, they tended to transform into a pair of carbonyl groups as shown in Fig. 3e, which was also reported by Abolfath [26]. With regard to the paired carbonyl groups, one carbonyl group was rearranged with the C-CO bond of another carbonyl group and became an over-coordinated epoxide group, releasing a CO molecule, as shown in Fig. 3d and Fig. 3f.

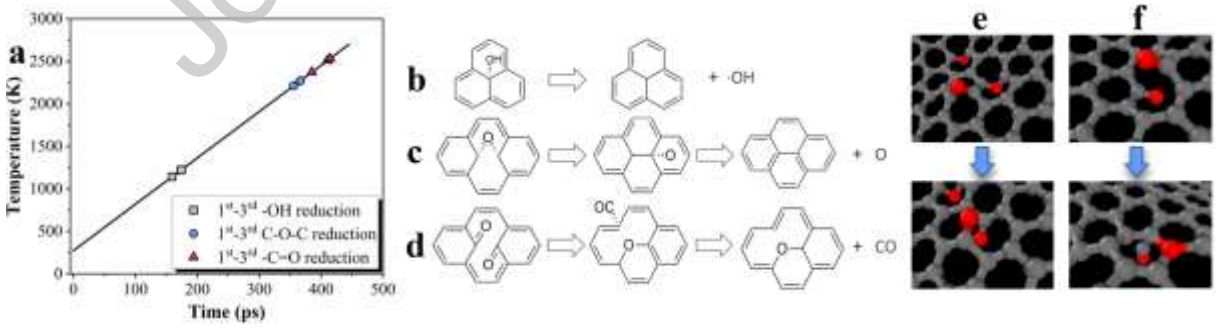

Fig. 3. (a) Simulation time-temperature profile for different OFGs in direct heating simulation. (b-c) Proposed reduction pathways for (b) hydroxyl, (c) epoxide, and (d) paired carbonyl groups. (e) The transformation of linked epoxide groups to paired carbonyl groups. (f) The transformation of paired carbonyl groups to over-coordinated epoxide group (grey for carbon atoms and red for oxygen atoms).

The microwave-assisted reduction of annealed GO was also simulated using localized heating fashion to mimic different heating rates introduced by different microwave powers, as illustrated in

Fig. 4. At low microwave power, the annealed GO sheet was hardly reduced and most of the OFGs remained intact, as shown in Fig. 4a. With increasing microwave power, the extent of deoxygenation was enhanced, as exemplified in Fig. 4b and Fig. 4c. Specifically, only 3.7% of the oxygen atoms were removed at low power microwave irradiation, which were far less than 49.8% at medium power and 83.5% at high power, as shown in Fig. 4d. The reason for the poor reduction at low microwave power was that the kinetic energy of the charged carbon atoms was dissipated into GO layers rather than being converted into localized overheating around OFGs. It is worth mentioning that at high microwave power, most of the OFGs were deoxygenated but the carbon skeleton was significantly damaged since more structural voids were formed during microwave irradiation, as shown in Fig. 4c. Compared to 0.04% at low microwave power and 7.5% at medium microwave power, 14.5% of the carbon atoms were removed at high microwave power, as shown in Fig. 4e. These simulation results supported that a high microwave power (800 W in this work) could lead to the effective deoxygenation of the OFGs and the formation of voids on the backbone. The extent of deoxygenation of OFGs at different microwave power levels was corroborated by further exposing the MWrGO samples to microwave irradiation at 800 W (Fig. S6). Since more OFGs were already deoxygenated at higher power levels, the MWrGO-800W sample showed less Joule heating when re-heated at the same microwave power level, which further validated the proposed decomposition/deoxygenation model.

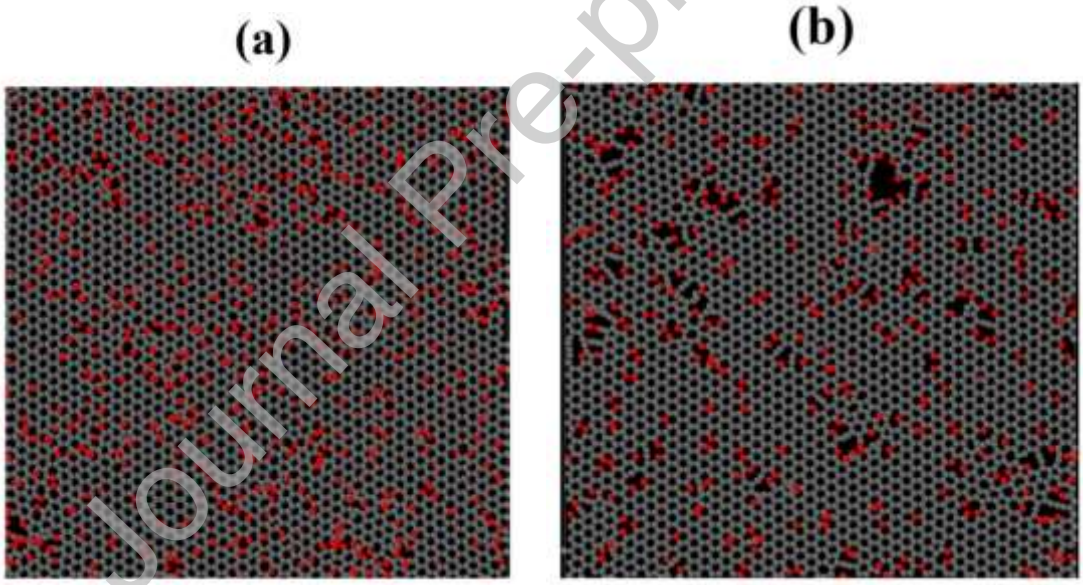

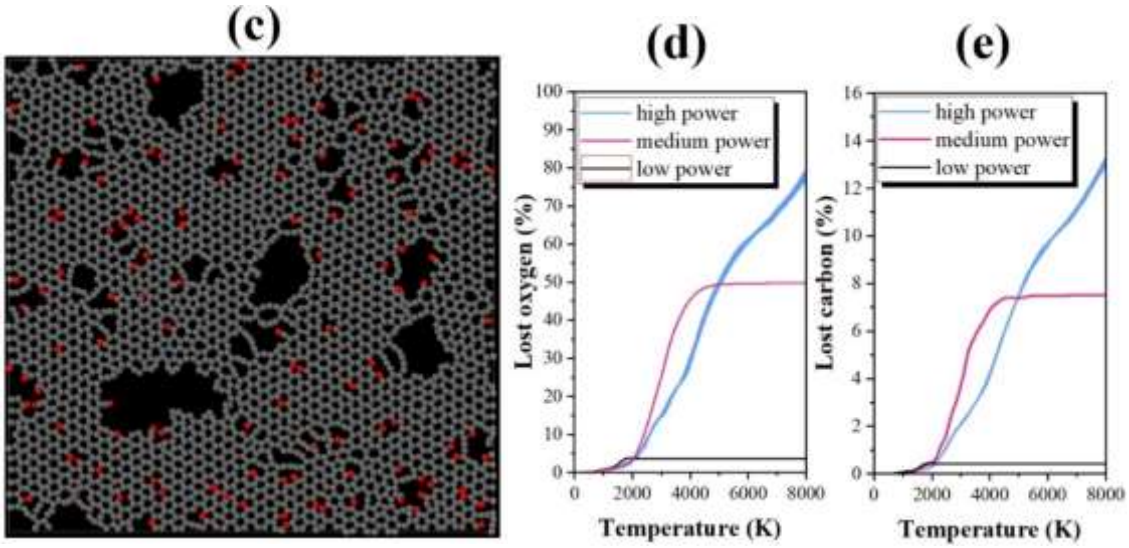

Fig. 4. The simulation results of MWrGO after microwave irradiation at (a) low power, (b) medium power and (c) high power. (d-e) Removed oxygen and carbon atoms on GO after microwave irradiation at different power levels.

3.3. The MWrGO characterization

Raman spectroscopy provides insights into structural evolutions relating to lattice disorder due to its unique phonon interaction with carbon hexagonal structure. All Raman spectra of MWrGO exhibit four characteristic peaks; D peak at ~1350 cm^{-1}, G peak at ~1580 cm^{-1}, 2D peak at ~2690 cm^{-1}, and 2D' at ~3240 cm^{-1} (Fig. 5a). The intensity ratio between D peak and G peak, i.e. I_D/I_G, has been intensively utilized as a measure of structural disorder in rGO and as a direct indicator for the extent of recovery of crystalline aromaticity. However, this empirical measuring tool, i.e. I_D/I_G, may give contradictory results on rGO synthesized by various methods, such as chemically/thermally treated rGO [31-34]. After being reduced from its GO precursors, an increased I_D/I_G may be observed for rGO instead of a decreased I_D/I_G. The unreliability of this empirical I_D/I_G is attributed to the superposition of G peak and D' peak, the latter of which generally appears at the high-Raman-shift shoulder of G peak. Due to the additional intensity contribution of D' peak to the observed apparent G peak (denoted as G_{App}, hereafter), the empirical I_D/I_G ratio is actually the intensity ratio between D peak and G_{App} peak ($I_D/I_{G\text{-}App}$). Depending on the contribution of D' peak, $I_D/I_{G\text{-}App}$ may vary from sample to sample and thus gives inconsistent comparisons over rGO samples. Therefore, by subtracting the intensity contribution of D' peak from G_{App} peak, a modified measuring ratio between D' peak to the intrinsic G peak (denoted as $I_D/I_{G\text{-}in}$) was proposed to study the structural evolutions of MWrGO (Fig. S7).

The $I_D/I_{G\text{-}in}$ ratios of all the MWrGO samples were calculated in Table S1. It is seen that the $I_D/I_{G\text{-}in}$ ratio is increased from ~0 in the pristine graphite to 1.258 for the unannealed GO, indicating the transformation of sp^2 graphitic domains to sp^3 amorphous domains by introducing OFGs. After annealing treatment at 250 °C, the $I_D/I_{G\text{-}in}$ ratio was significantly reduced to 0.906, representing the partial recovery of conjugated graphitic structure. After microwave irradiation, the $I_D/I_{G\text{-}in}$ ratio of MWrGO decreased to 0.392 at 300 W, 0.251 at 500 W and further to 0.062 at 800 W, indicating an effective removal of OFGs at higher microwave power. In comparison with annealed GO, the unannealed GO showed poor reduction even at the highest microwave power of 800 W, which indicated the importance of annealing treatment which can convert GO from a poor microwave absorber to an extraordinary microwave absorber.

I_{2D}/I_G ratios and crystalline domain size (L_a) are other indicators for the quality of synthesized rGO. The larger the values of I_{2D}/I_G ratios and L_a, the higher quality of rGO. Fig. 5b depicts the I_{2D}/I_G ratios as a function of L_a on MWrGO samples in comparison with CVD-graphene and dispersed graphene. Among MWrGO samples, MWrGO-800W exhibited the largest values of I_{2D}/I_G ratio and L_a, representing less OFGs on graphene plane (Table S1). The aforementioned Raman analysis revealed that highest-quality MWrGO could be obtained using 800 W of microwave power and this is consistent with the RMD simulation results. The most attractive MWrGO-800W was then selected as a representative for further characterization.

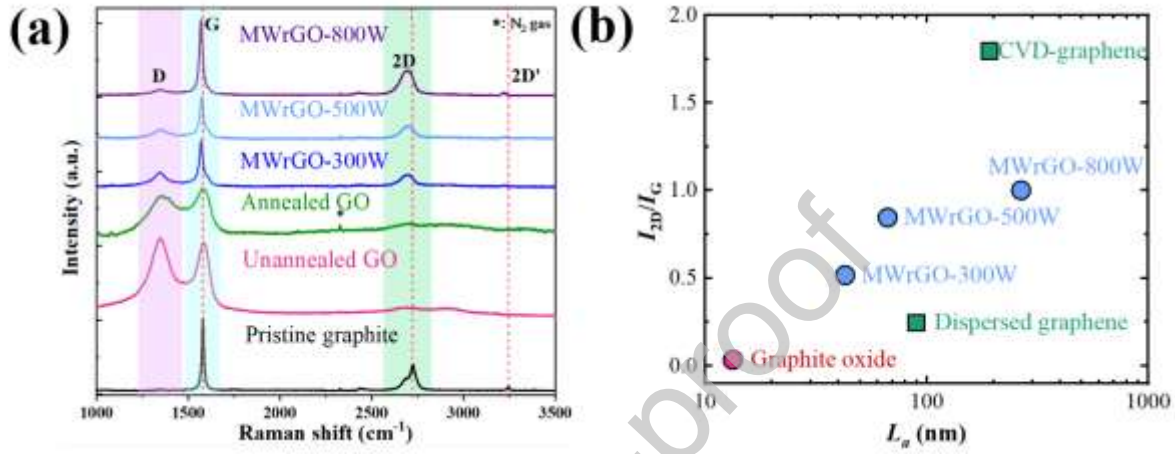

Fig. 5. (a) Raman spectra of MWrGO in comparison with pristine graphite, unannealed GO, and annealed GO. (b) I_{2D}/I_G intensity versus the crystalline domain sizes (L_a) for MWrGO, CVD-graphene and dispersed graphene (the latter two were added for comparison from ref. [17]).

The quantified amounts of OFGs on pristine graphite, unannealed GO, annealed GO and MWrGO-800W were determined using XPS (Fig. 6, Table S2). The XPS C1s spectra featured the following bands: non-oxygenated ring C-C at 284.48 eV, C-O at 285.98 eV, C=O at 287.48 eV, O-C=O at 288.98 eV, and π-π* shake-up peak at 291.28 eV. The intensities of the OFGs on the unannealed GO became significant after the modified Hummer's method and then were effectively reduced after the annealing process and microwave irradiation. The appearance of π-π* shake-up peak and the increase in the C-C band intensity for the annealed GO and the MWrGO-800W confirmed: (i) the effective reduction of the oxygenated graphene sheets during the annealing treatment at 250 °C and (ii) the further removal of OFGs upon microwave irradiation. Similar corroborative conclusions can also be drawn based on the structural, compositional, and thermal analysis using XRD, FTIR, TGA, and nitrogen adsorption-desorption isotherms, which are detailed in Fig. S8-S11. In short summary, the MWrGO-800W exhibited a high C/O ratio of 14.29 and a high specific surface area (S_{BET}) of 310.24 $m^2 g^{-1}$ (Table S2 and Fig. S11).

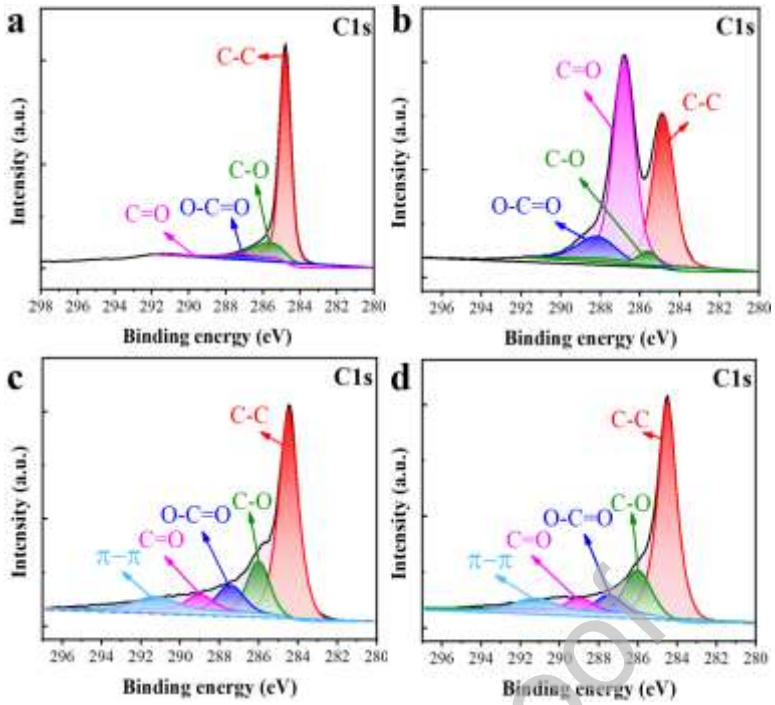

Fig. 6. The XPS C1s spectra of (a) pristine graphite, (b) unannealed GO, (c) annealed GO, and (d) MWrGO-800W.

Generally, a high electronic conductivity of graphene is closely related to the perfection of carbon hexagonal structures. GO is electrically insulated because the extended π-π* electronic conjugated network is damaged by the presence of OFGs. As shown in Fig. S12, the electronic conductivity of the unannealed GO (1.83×10^{-2} S m^{-1}) was much inferior than that of the pristine graphite (851.2 S m^{-1}), implying that the transportation of π electrons was blocked by OFGs. After annealing treatment and microwave-assisted reduction, the electronic conductivities of annealed GO and MWrGO-800W yielded values of 268.9 S m^{-1} and 761.4 S m^{-1}, respectively, which are excellent compared to literature values (Table S3). There was a direct relation noticed between the electronic conductivity and the C/O ratios of the samples (Fig. S13), indicating that the removal of OFGs can enhance the free transportation of π electrons on graphene nanosheets.

3.4. The applications of MWrGO in LIBs

As discussed above, the high S_{BET} (310.24 m^2 g^{-1}) and the high electronic conductivity (761.4 S m^{-1}) can enable the MWrGO-800W as an excellent electroactive material in anode and a conductive additive in cathode for LIBs due to (i) the sufficient uptake sites for Li ions, (ii) the formation of elastic and highly conductive 3-dimensional network, (iii) the enhanced lithium ion mobility through large-size voids [6]. This is further investigated here.

MWrGO-800W anode exhibited a discharge capacity of 1523.9 mAh g^{-1} and a charge capacity of 755.1 mAh g^{-1} in the initial cycle, yielding a coulombic efficiency of only 49.5% (Fig. 7a). The large initial discharge capacity mainly involved the irreversible capacity caused by the formation of a passivating solid electrolyte interphase (SEI) on the graphene flakes and the reversible capacity caused by the intercalation process of lithium ions [35]. Among them, the reversible intercalation process of lithium ions was consisted of the electrochemical lithiation/delithiation process (<0.5 V) and the Faradic capacitance on the structural voids of the graphene flakes (>0.5 V) [4].

A stable discharge capacity of ~750.0 mAh g^{-1} was attained subsequently for the MWrGO-800W anode, corresponding to a high stoichiometric Li_xC_6 (X≈2.0) (Fig. 7b). In contrast with crystalline graphite in which each graphitic flake is thought to only accommodate a single layer of Li ions, well-exfoliated MWrGO-800W seems to be capable to uptake a layer of Li ions on both sides of graphene flake. This enables the specific capacity of MWrGO-800W to be almost double that of crystalline graphite (372 mAh g^{-1}). Moreover, the structural voids on the MWrGO-800W flakes can function as additional Li^+ storage sites, further increasing the attainable capacity. The low coulombic efficiency of 49.54% in the initial cycle progressively increased to 96.91% at 5th cycle and then stabilized at around 100%, indicating that the SEI formed in the first 5 cycles was stable and the intercalation/deintercalation process was reversible. The intercalation/deintercalation behavior of MWrGO-800W with Li ions was further studied using CV test between 0.01-2.5 V (Fig. S14). In the first cathodic scan, a strong reduction peak was observed at 0.66 V and was attributed to the formation of SEI. However, this reduction peak disappeared in the subsequent cathodic scans, which was indicative of the SEI stability. In the initial five scans, MWrGO-800W electrode featured a reduction peak at 0.02 V and an oxidation peak at 0.19 V, which exhibited an excellent consistency in shape and were assigned to the intercalation/deintercalation of Li ions in a manner reflecting Li_xC_6 bulk storage. Overall, the excellent consistency of CV test indicated the good reversibility of the MWrGO-800W anode.

With stepwise increasing the current densities to 10 A g^{-1}, the capacities of MWrGO-800W were declined to 120 mAh g^{-1} (Fig. 7c). The diminishing capacities of MWrGO-800W can be attributed to the increased polarization at high current densities. More notably, the exceptional capacity of 120 mAh g^{-1} at the super-high current density of 10 A g^{-1} was indicative of the presence of structural voids formed during microwave irradiation, which provided channels for faster diffusive motion of Li^+ ion [6]. A remarkable capacity of 750 mAh g^{-1} was retained at 0.1 A g^{-1} immediately after being charge/discharged at 10 A g^{-1}, indicating the robust microstructure of MWrGO-800W and the stable SEI formed [36]. The capacities of MWrGO-300W, MWrGO-500W and MWrGO-800W were also compared in Fig. S15. In contrast with 750.0 mAh g^{-1} for the MWrGO-800W anode, the lower capacities of ~520.0 mAh g^{-1} and ~400.0 mAh g^{-1} were achieved for MWrGO-500W and MWrGO-300W, respectively, which could be ascribed to (i) the less accessible sites for Li ions due to the occupancy of residual OFGs, and (ii) the less structural voids formed at lower microwave powers. Thus, the electrochemical evaluation of MWrGO samples further agrees with the RMD simulations and Raman results.

The improvement on the use of MWrGO-800W in LCO electrode (LCO-MWrGO) was studied in comparison with the counterpart containing CNT (LCO-CNT). Compared with LCO-MWrGO which showed a smooth capacity decay over 100 cycles, LCO-CNT suffered from a rapid capacity decay in the first 20 cycles, followed by a smooth capacity decay in the successive cycles (Fig. 7d). After 100 cycles, the capacity retentions were 87.7% for LCO-MWrGO and 74.6% for LCO-CNT relative to their initial capacities. The higher capacity retention of LCO-MWrGO was ascribed to the sheet characteristic of MWrGO. The graphene sheets could wrap the LCO particles and prevent them from disintegration (Fig. 8 and Fig. S16). In this scenario, more LCO particles were able to firmly embed in the sponge-like MWrGO architecture and continually contribute to the overall capacity even though the LCO particles experienced expansion and contraction along *C* axis during the lithiation/delithiation process [37, 38]. Nevertheless, as expected the tube-shape CNT cannot provide

buffering volume for LCO particles, thereby leading to electrode disintegration and capacity fading upon long-term cycling.

The LCO-MWrGO showed a similar rate capability as LCO-CNT at low current rate (<1 C) whilst it exhibited a superior rate performance at high current rates >2 C (Fig. 7e). Specifically, the capacity retention of LCO-MWrGO was ~70% at 10 C, which was much more extraordinary than ~0% of LCO-CNT. The high capacity retention of LCO-MWrGO at high current rate can be attributed to (i) the effective plane-to-point contact model in which the spherical-shape LCO particles come in contact with planar graphene flakes, providing more contact points [39], (ii) the higher utilization efficacy of the carbon atoms on the planar graphene flakes [39], (iii) the porous structure of MWrGO which can facilitate the absorption and retention of electrolyte solution, providing an intimate contact between active material and electrolyte [20, 40]. When the current rate was returned to 0.1 C, a slightly higher capacity of LCO-MWrGO, i.e. ~130 mAh g^{-1}, was achieved in comparison to that of ~125 mAh g^{-1} in LCO-CNT. It is worth pointing out that the content of MWrGO (1 wt%) used in LCO-MWrGO is less than that of CNT used (3 wt%) in LCO-CNT, indicating that higher volumetric capacity can be realized for LCO-MWrGO cathode system.

EIS measurements were conducted to investigate the reasons why LCO-MWrGO exhibited improved electrochemical properties over LCO-CNTs, particularly at high current rates (Fig. 7f and Table S4). All the curves comprise a single semicircle and a quasi linear tail which are ascribed to the charge transfer process and Li ion diffusion in the solid phase of the electrode, respectively. After 100 cycles, the R_s for the LCO-CNTs exhibited greater increase than that for LCO-MWrGO, which indicated the side reactions of the electrolyte could be suppressed by the graphene hence lower electrlyte resistance observed. It is worth noting that the R_{ct} of LCO-MWrGO was much smaller than that of LCO-CNTs regardless of cycling test. The effectiveness of MWrGO in improving interfacial charge transfer kinetics manifests itself when comparing charge transfer resistances at solid particles. R_{ct} is the main factor to affect the electrode kinetics during rate capability test, especially at high current rate. The small values of LCO-MWrGO can be attributed to the excellent electronic conductivity and the improved contact area of MWrGO.

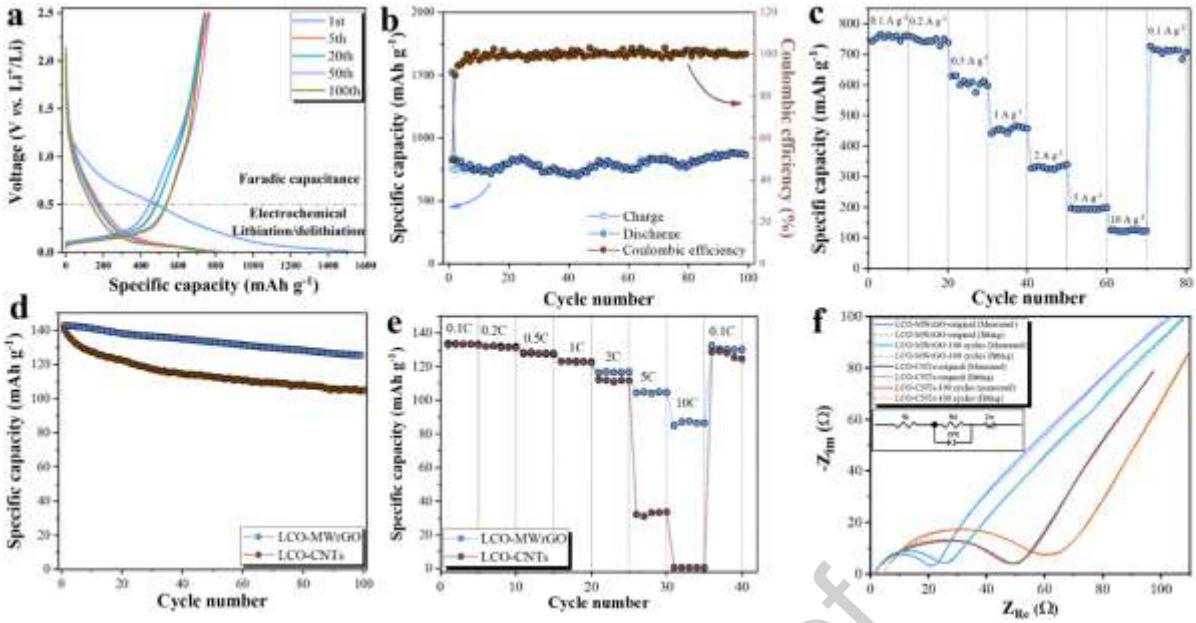

Fig. 7. (a) The galvanostatic charge/discharge curves of MWrGO-800W anode at the current density of 0.2 A g^{-1}. (b) The cycling performances of MWrGO-800W anode at 0.2 A g^{-1}. (c) Rate capability of MWrGO-800W anode. (d) The cycling performances of LCO-MWrGO and LCO-CNTs at C/5 (1C=140.0 mAh g^{-1}). (e) The rate capability comparison of LCO-MWrGO and LCO-CNTs. (f) Nyquist plots of LCO-MWrGO and LCO-CNTs before and after 100 cycles with the equivalent circuit in the inset, where R_s represents the electrolyte resistance, R_{ct} represents the charge transfer resistance, CPE stands for constant phase element and Z_w is the Warburg impedance, which is attributed to the Li diffusion on LCO particles.

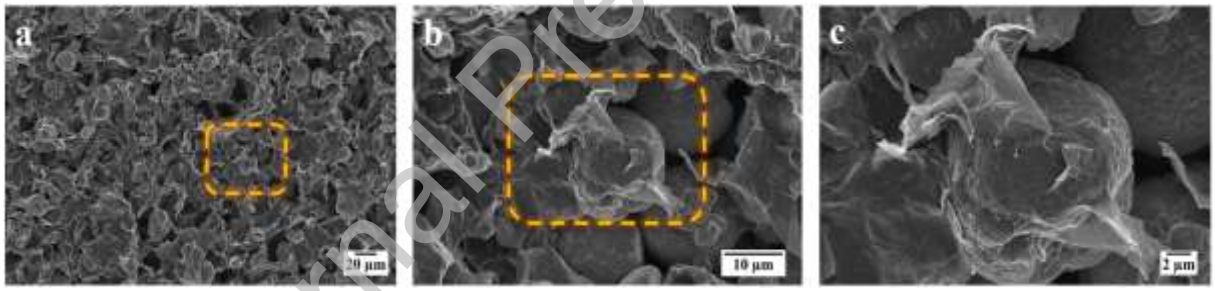

Fig. 8. FEGSEM images of LCO-MWrGO cathode at (a) lower magnification, (b) medium magnification and (c) higher magnification.

4. Conclusions

In summary, this work demonstrated the feasibility of microwave reduction of solid-state GO to synthesize MWrGO within seconds. RMD simulations suggested that different microwave powers could be used to tailor the quality of MWrGO product. The reduction mechanisms of different OFGs were also proposed based on RMD simulations. Through comprehensive structural and compositional characterization, high-quality MWrGO was successfully produced using the microwave power of 800 W. A modified $I_D/I_{G\text{-}in}$ Raman metric was shown to give a more reliable structural evaluation for MWrGO by deducting the intensity contribution of D peak from the apparent G peak. In LIB applications, the anode made of MWrGO-800W delivered a high capacity of ~750.0 mAh g^{-1} with near-zero capacity loss after 100 cycles. Additionally, a highly conductive 3D network constructed by porous MWrGO-800W provided $LiCoO_2$ with a high capacity retention of ~70% at the high current rate of 10 C, which is promising for power-oriented cathode. Thus, the microwave-

assisted reduction of GO provides a rapid way to produce high-quality graphene for energy storage devices at an affordable cost and at bulk scale.

Conflicts of interest

There are no conflicts to declare.

Acknowledgements

This work was supported by The Engineering and Physical Sciences Research Council [grant number EP/N010493/1]. The authors also appreciated the help of Loughborough Materials Characterization Center. Specifically, Dr. Zhaoxia Zhou is gratefully acknowledged for the assistance with HR-TEM characterization.

References

[1] M.D. Stoller, S. Park, Y. Zhu, J. An, R.S. Ruoff, Graphene-based ultracapacitors, Nano Lett. 8(10) (2008) 3498-3502.

[2] J. Park, A. Akbari-Sharbaf, S. Ezugwu, R. Bauld, G. Fanchini, Direct synthesis of highly conducting graphene nanoribbon thin films from graphene ridges and wrinkles, Acta Mater. 107 (2016) 96-101.

[3] H. Hu, Z. Zhao, Q. Zhou, Y. Gogotsi, J. Qiu, The role of microwave absorption on formation of graphene from graphite oxide, Carbon 50(9) (2012) 3267-3273.

[4] R. Liu, Y. Zhang, Z. Ning, Y. Xu, A catalytic microwave process for superfast preparation of high-quality reduced graphene oxide, Angew. Chem., Int. Ed. 56(49) (2017) 15677-15682.

[5] D. Ma, Y. Li, M. Wu, L. Deng, X. Ren, P. Zhang, Enhanced cycling stability of Li-rich nanotube cathodes by 3D graphene hierarchical architectures for Li-ion batteries, Acta Mater. 112 (2016) 11-19.

[6] E. Alsharaeh, F. Ahmed, Y. Aldawsari, M. Khasawneh, H. Abuhimd, M. Alshahrani, Novel synthesis of holey reduced graphene oxide (HRGO) by microwave irradiation method for anode in lithium-ion batteries, Sci. Rep. 6 (2016) 29854.

[7] A.M. Schwenke, S. Hoeppener, U.S. Schubert, Synthesis and modification of carbon nanomaterials utilizing microwave heating, Adv. Mater. 27(28) (2015) 4113-4141.

[8] P. Ranjan, S. Agrawal, A. Sinha, T.R. Rao, J. Balakrishnan, A.D. Thakur, A Low-Cost Non-explosive Synthesis of Graphene Oxide for Scalable Applications, Sci. Rep. 8(1) (2018) 12007.

[9] H.N. Tien, V.H. Luan, T.V. Cuong, B.S. Kong, J.S. Chung, E.J. Kim, S.H. Hur, Fast and simple reduction of graphene oxide in various organic solvents using microwave irradiation, J. Nanosci. Nanotechno. 12(7) (2012) 5658-5662.

[10] W. Chen, L. Yan, P.R. Bangal, Preparation of graphene by the rapid and mild thermal reduction of graphene oxide induced by microwaves, Carbon 48(4) (2010) 1146-1152.

[11] H.C. Schniepp, J. Li, M.J. McAllister, H. Sai, M. Herrera-Alonso, D.H. Adamson, R.K. Prud'homme, R. Car, D.A. Saville, I.A. Aksay, Functionalized single graphene sheets derived from splitting graphite oxide, J. Phys. Chem. B 110(17) (2006) 8535-8539.

[12] X. Li, G. Zhang, X. Bai, X. Sun, X. Wang, E. Wang, H. Dai, Highly conducting graphene sheets and Langmuir–Blodgett films, Nat. Nanotechnol. 3 (2008) 538.

[13] Y. Zhu, S. Murali, M.D. Stoller, A. Velamakanni, R.D. Piner, R.S. Ruoff, Microwave assisted exfoliation and reduction of graphite oxide for ultracapacitors, Carbon 48(7) (2010) 2118-2122.

[14] S. Park, S. Bak, K. Kim, J. Jegal, S. Lee, J. Lee, K. Kim, Solid-state microwave irradiation synthesis of high quality graphene nanosheets under hydrogen containing atmosphere, J. Mater. Chem. 21(3) (2011) 680-686.

[15] W. Jiang, C. Yang, G. Chen, X. Yan, S. Chen, B. Su, Z. Liu, J. Tian, Preparation of high-quality graphene using triggered microwave reduction under an air atmosphere, J. Mater. Chem. C 6(7) (2018) 1829-1835.

[16] E.M. Moon, C. Yang, V.V. Yakovlev, Microwave-induced temperature fields in cylindrical samples of graphite powder–Experimental and modeling studies, Int. J. Heat Mass Transfer 87 (2015) 359-368.

[17] D. Voiry, J. Yang, J. Kupferberg, R. Fullon, C. Lee, H.Y. Jeong, H.S. Shin, M. Chhowalla, High-quality graphene via microwave reduction of solution-exfoliated graphene oxide, Science 353(6306) (2016) 1413-1416.

[18] V.V. Chaban, O.V. Prezhdo, Microwave reduction of graphene oxide rationalized by reactive molecular dynamics, Nanoscale 9(11) (2017) 4024-4033.

[19] S. Petnikota, N.K. Rotte, V.V. Srikanth, B.S. Kota, M. Reddy, K.P. Loh, B. Chowdari, Electrochemical studies of few-layered graphene as an anode material for Li ion batteries, J. Solid State Electrochem. 18(4) (2014) 941-949.

[20] Y. Shi, L. Wen, S. Pei, M. Wu, F. Li, Choice for graphene as conductive additive for cathode of lithium-ion batteries, J. Energy Chem. 30 (2019) 19-26.

[21] W.S. Hummers, R.E. Offeman, Preparation of graphitic oxide, J. Am. Chem. Soc. 80(6) (1958) 1339-1339.

[22] D.C. Marcano, D.V. Kosynkin, J.M. Berlin, A. Sinitskii, Z. Sun, A. Slesarev, L.B. Alemany, W. Lu, J.M. Tour, Improved synthesis of graphene oxide, ACS Nano 4(8) (2010) 4806-4814.

[23] C. Bao, S. Bi, H. Zhang, J. Zhao, P. Wang, C.Y. Yue, J. Yang, Graphene oxide beads for fast clean-up of hazardous chemicals, J. Mater. Chem. A 4(24) (2016) 9437-9446.

[24] S. Plimpton, Fast parallel algorithms for short-range molecular dynamics, J. Comput. Phys. 117(1) (1995) 1-19.

[25] A. Stukowski, Visualization and analysis of atomistic simulation data with OVITO–the Open Visualization Tool, Modell. Simul. Mater. Sci. Eng. 18(1) (2009) 015012.

[26] R.M. Abolfath, K. Cho, Computational studies for reduced graphene oxide in hydrogen-rich environment, J. Phys. Chem. A 116(7) (2012) 1820-1827.

[27] A.C. Van Duin, S. Dasgupta, F. Lorant, W.A. Goddard, ReaxFF: a reactive force field for hydrocarbons, J. Phys. Chem. A 105(41) (2001) 9396-9409.

[28] J.M. Kim, D. Ko, J. Oh, J. Lee, T. Hwang, Y. Jeon, W. Hooch Antink, Y. Piao, Electrochemically exfoliated graphene as a novel microwave susceptor: the ultrafast microwave-assisted synthesis of carbon-coated silicon-graphene film as a lithium-ion battery anode, Nanoscale 9(40) (2017) 15582-15590.

[29] Q. Qiao, C. Liu, W. Gao, L. Huang, Graphene oxide model with desirable structural and chemical properties, Carbon 143 (2019) 566-577.

[30] A. Bagri, C. Mattevi, M. Acik, Y.J. Chabal, M. Chhowalla, V.B. Shenoy, Structural evolution during the reduction of chemically derived graphene oxide, Nat. Chem. 2(7) (2010) 581.

[31] D. Yang, A. Velamakanni, G. Bozoklu, S. Park, M. Stoller, R.D. Piner, S. Stankovich, I. Jung, D.A. Field, C.A. Ventrice, R.S. Ruoff, Chemical analysis of graphene oxide films after heat and chemical treatments by X-ray photoelectron and Micro-Raman spectroscopy, Carbon 47(1) (2009) 145-152.

[32] A.A.K. King, B.R. Davies, N. Noorbehesht, P. Newman, T.L. Church, A.T. Harris, J.M. Razal, A.I. Minett, A new raman metric for the characterisation of graphene oxide and its derivatives, Sci. Rep. 6 (2016) 19491.

[33] S. Stankovich, D.A. Dikin, R.D. Piner, K.A. Kohlhaas, A. Kleinhammes, Y. Jia, Y. Wu, S.T. Nguyen, R.S. Ruoff, Synthesis of graphene-based nanosheets via chemical reduction of exfoliated graphite oxide, Carbon 45(7) (2007) 1558-1565.

[34] A. Anshuman, S. Saremi-Yarahmadi, B. Vaidhyanathan, Enhanced catalytic performance of reduced graphene oxide-TiO_2 hybrids for efficient water treatment using microwave irradiation, RSC Adv. 8(14) (2018) 7709-7715.

[35] J. Hassoun, F. Bonaccorso, M. Agostini, M. Angelucci, M.G. Betti, R. Cingolani, M. Gemmi, C. Mariani, S. Panero, V. Pellegrini, B. Scrosati, An advanced lithium-ion battery based on a graphene anode and a lithium iron phosphate cathode, Nano Lett. 14(8) (2014) 4901-4906.

[36] K. Fu, Y. Wang, C. Yan, Y. Yao, Y. Chen, J. Dai, S. Lacey, Y. Wang, J. Wan, T. Li, Graphene oxide-based electrode inks for 3D-printed lithium-ion batteries, Adv. Mater. 28(13) (2016) 2587-2594.

[37] Y. Takahashi, N. Kijima, K. Dokko, M. Nishizawa, I. Uchida, J. Akimoto, Structure and electron density analysis of electrochemically and chemically delithiated $LiCoO_2$ single crystals, J. Solid State Chem. 180(1) (2007) 313-321.

[38] P. Stein, A. Moradabadi, M. Diehm, B.-X. Xu, K. Albe, The influence of anisotropic surface stresses and bulk stresses on defect thermodynamics in $LiCoO_2$ nanoparticles, Acta Mater. 159 (2018) 225-240.

[39] F. Su, Y. He, B. Li, X. Chen, C. You, W. Wei, W. Lv, Q. Yang, F. Kang, Could graphene construct an effective conducting network in a high-power lithium ion battery?, Nano Energy 1(3) (2012) 429-439.

[40] J.K. Hong, J.H. Lee, S.M. Oh, Effect of carbon additive on electrochemical performance of $LiCoO_2$ composite cathodes, J. Power Sources 111(1) (2002) 90-96.